Supplementary Information

Compact modeling of hysteresis in Organic Thin-Film Transistors ⋆

A. Romero[a], J. A. Jiménez-Tejada[a,*], R. Picos[b], D. Lara[a], J.B. Roldán[c], M.J. Deen[d]

[a]*Departamento de Electrónica y Tecnología de Computadores, CITIC-UGR, Universidad de Granada, Granada 18071, Spain*
[b]*Department of Industrial Engineering and Construction, Universitat de les Illes Balears, Palma 07122, Illes Balears, Spain*
[c]*Departamento de Arquitectura y Tecnología de Computadores, CITIC-UGR, Universidad de Granada, Granada 18071, Spain*
[d]*Department of Electrical and Computer Engineering, McMaster University, 1280 Main Street West, Hamilton, Ontario L8S 4K1, Canada*

Contents

⋆The authors acknowledge support from the project PID2022-139586NB-44 funded by MCIN/AEI/10.13039/501100011033 and by European Union NextGenerationEU/PRTR.

*Corresponding author, tejada@ugr.es

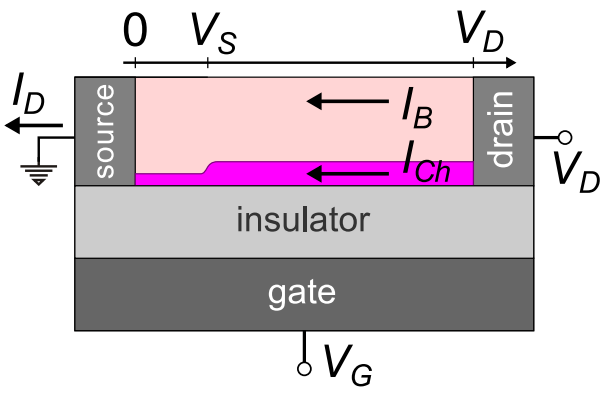

Figure S1: Bottom-contact OTFT showing the conduction I_{Ch} and depletion I_B current components.

S1. Depletion region. Model

Figure S1 shows a cross sectional view of an Organic Thin-Film Transistor (OTFT) structure. The source terminal voltage is zero and V_D and V_G are the drain and gate terminal voltages, respectively. V_S is the voltage drop at the source contact (the contact region is exaggerated for clarity). The electric current flowing between drain and source terminals I_D is composed of the field-effect (channel) current I_{Ch} flowing in the accumulation layer, and the bulk current I_B [1]:

$$I_D = I_B + I_{Ch}. \tag{S1}$$

In the depletion (cut-off) region, $I_{Ch} \ll I_B$ and $I_D \simeq I_B$. In sub-threshold or over-threshold conditions, $I_B \ll I_{Ch}$ and $I_D \simeq I_{Ch}$, which is the component described in the main text. In order to ensure a smooth transition from depletion to conduction, (S1) can be written as:

$$\begin{aligned} &I_D = I_B \left[1 + \left(\frac{I_{Ch}}{I_B}\right)^s\right]^{1/s}, \\ &\forall s \in \mathbb{Z} : s > 0 \end{aligned} \tag{S2}$$

where s is a free parameter employed to control the transition smoothness [2], and it is incorporated in the set of parameters that define the individual (18).

S2. Measurement protocol

Fig. S2 shows the time sequences of V_D and V_G applied to the p-type TFT and used in the simulation. This sequence is different for the three experiments analyzed in this work: output characteristics (Fig. S2a), transfer characteristics (Fig. S2b), and current transients (Fig. S2c).

S2.1. Output characteristics

The beginning of a combined forward-backward (FB) $I_D - V_D$ curve is characterized by the bias point $V_D = 0\,\mathrm{V}$ and $V_G = V_{G_m}$, where $m = 1...N_G$ and N_G is the number of discrete values for V_G in the $I_D - V_G$ experiment. Under an initialization process, these two voltages, $V_D = 0\,\mathrm{V}$ and $V_G = V_{G_m}$, are kept constant during a waiting time or hold-time $t_{hold} = 3$ s (Fig. S2a). During t_{hold}, traps are charged following equation (14), or (15) in its discrete form, re-written here for the sake of clarity:

$$\begin{aligned} Q_{tL}(t_j) &= \sum_{r=1}^{n_{traps}} Q_{tL_r}(t_j), \\ Q_{tL_r}(t_j) &= Q_{tL_r}(t_{j-1}) e^{-\frac{t_j - t_{j-1}}{\tau_r}} + Q_{t0_r}(1 - e^{-\frac{t_j - t_{j-1}}{\tau_r}}), \\ Q_{t0_r} &= q N_{T_r} y_G. \end{aligned} \tag{S3}$$

In the simulation, we consider that Q_{t0_r} increases linearly with V_G. If V_G increases in constant steps, then $Q_{t0_r}(V_{G_m}) = m \times Q_{t0_r}(V_{G_1})$ where $Q_{t0_r}(V_{G_1}) = Q_{tL,1}$ (the fitting parameter x_{17} in Table 1).

After this hold-time, V_D is swept and trapping and de-trapping are described with equation (16) (or (17) in its discrete form).

S2.2. Transfer characteristics

The drain voltage is kept constant at $V_D \neq 0$ (Fig. S2b). The drain current is also different from zero during the whole experiment. Thus, trapping and de-trapping are always described with equation (16) (or (17) in its discrete form). The value of V_G for $t < 0\,\mathrm{s}$ is at the deep sub-threshold condition. Thus, there are no free carriers available to fill the traps, and the initial trapped charge density is zero.

S2.3. Transient behavior

Like in the transfer characteristics, the drain voltage is kept constant at a value different from zero (Fig. S2c), and the drain current is different from zero during the whole experiment. Thus, trapping and de-trapping is always described with equation (16) (or (17) in its discrete form). The value of V_G for $t < 0\,\mathrm{s}$ is for a deep sub-threshold condition. Thus, there are no free carriers available to fill the traps, and the initial trapped charge density is zero.

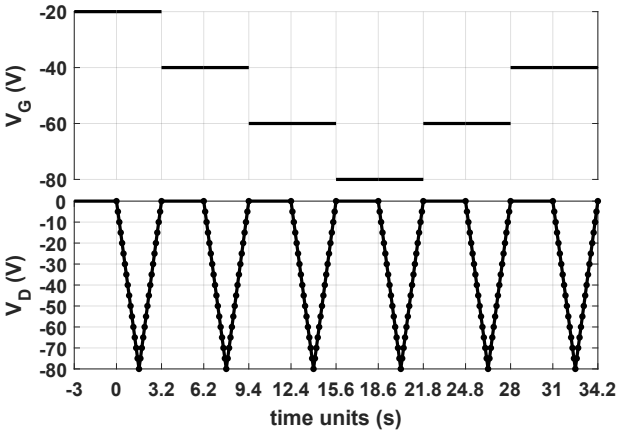

(a)

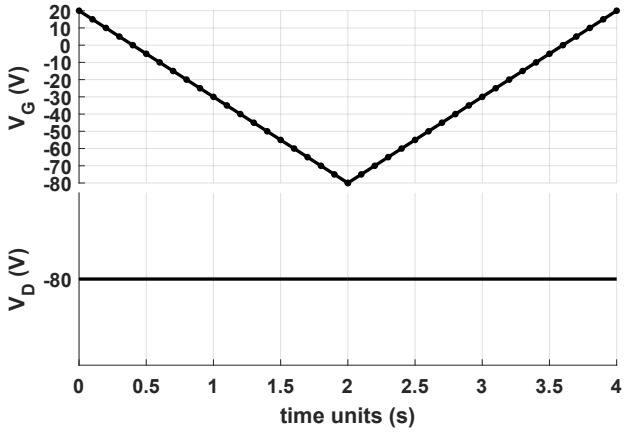

(b)

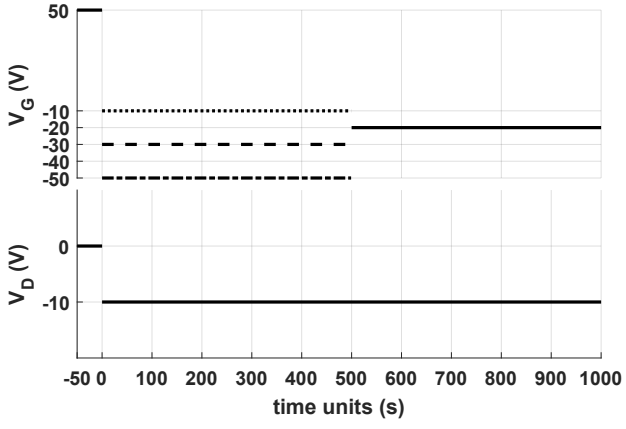

(c)

Figure S2: Measurement protocol describing the temporal sequence of the gate and drain voltages used during the measurement [3, 4] and simulation of (a) output characteristics, (b) transfer characteristics and (c) current transients.

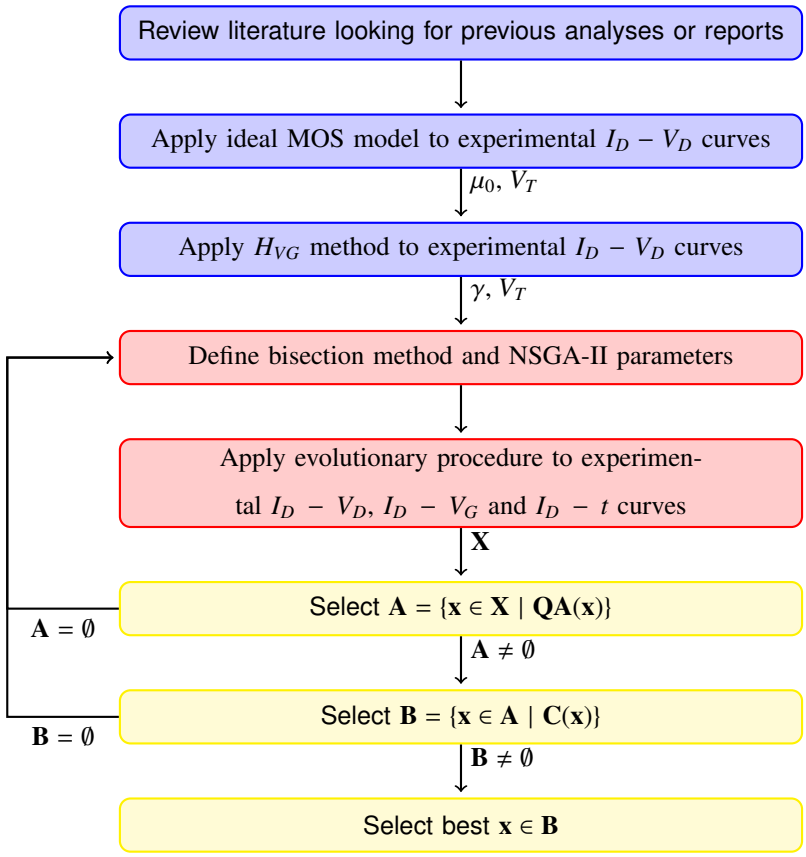

Figure S3: Flow chart of the decision-making process followed by the authors (DMs) in this work.

S3. Decision-making process

The decision-making process followed by the authors is described in the following sections and represented in Fig. S3. Note that the full description of the evolutionary extraction procedure is found in Ref. [5] and complemented in the main paper.

S3.1. Review of the literature

In the first place, a comprehensive review of the literature is performed in order to collect previous analyses or reports of the target device. Also, information about devices sharing characteristics with the target one is highly valuable. In summary, the main goal of this is to gather as much information as possible to help Decision-Makers (DMs) in the decision-making.

S3.2. Use of ideal MOS model

The ideal MOS model is applied to the device experimental $I_D - V_D$ curves to extract the device μ_0 and V_T parameters. DMs use these extracted μ_0 and V_T values to define the search space of both parameters in the evolutionary

procedure. Note that both μ_0 and V_T estimations may differ from the real ones because the ideal MOS model does not include: the dependence of mobility with electric field, the effect of the contacts, or time variations of the threshold voltage caused by trapping effects.

S3.3. Use of H_{VG} method

The H_{VG} method [6] is applied to the device experimental $I_D - V_D$ curves to extract the device γ and V_T parameters. DMs use the extracted γ and V_T values to define the search space of both parameters in the evolutionary procedure. Also, in this case, both γ and V_T estimations may differ from the real ones because H_{VG} method neglects the voltage drop at the contact in order to determine these parameters, and V_T is assumed independent of time. Note that in OTFTs, the estimation of γ is only taken into account if it agrees with γ values associated to the crystalline-like behavior and a narrow distributions of the DOS of the device. On the contrary, this γ estimation is discarded.

S3.4. Evolutionary procedure configuration

Several configuration parameters must be defined to perform the parameter extraction. All of them are fully introduced and explained in Ref. [5]. It is of the utmost importance the definition of a proper individual x and fitness function O. Both of them are directly related to the target device that we aim to analyze. Once again, the definition of both x and O require a number of clarifications.

S3.4.1. Individual representation x

An individual x includes all the parameters needed to compute the device model [in the main text, the ones included in (1), (3), (6), (12) and (13), (15) and (17) and particularized to the three different experiments $I_D - V_D$, $I_D - V_G$ and $I_D - t$ (Table 1)]. The previous steps (study of the literature and use of the ideal MOS model, H_{VG} method, or other sequential methods [7, 8]) help DMs to achieve this purpose. In particular, they find an initial estimation of common parameters to the three experiments $I_D - V_D$, $I_D - V_G$ and $I_D - t$ (μ_0, γ and V_T). A valid parameter set configuration allows the procedure to converge to optimum solutions. If an optimal solution is not achieved, new parameter set configurations must be tried.

S3.4.2. Fitness function O

The fitness function O assigns a fitness value to each individual x for each one of the objectives defined in our MaOP [in the main text (20)]. Here, DMs are in charge of defining the objective functions that they want to optimize using x. In the main text, there are three objectives, all related to the minimization of the error between the experimental values of $I_D = I_D(V_G(t_j), V_D(t_j))$ taken in three different experiments ($I_D - V_D$, $I_D - V_G$ and $I_D - t$) and their estimation $\widehat{I_D}(V_G(t_j), V_D(t_j), x)$ calculated from (1), (3), (6), (12), (13), (15) and (17). The definition of O must agree with the device's properties. On the contrary, the procedure will not converge to optimum solutions. A full description of the fitness function can be found in [5]. In addition, the steps to configure O to different device's parameters and models are found in Ref. [9, 10].

S3.5. Parameter extraction

Once all parameters have been defined and the evolutionary procedure has been properly configured, the procedure aims to the best fitting with the different experimental $I_D = I_D(V_G(t_j), V_D(t_j))$ curves. After the evolutionary procedure execution, a set of potential solutions (**X**) are obtained.

S3.6. Quality of the result

DMs check and keep the solutions from **X** that fit well enough the experimental data. The procedures of checking the quality of a solution x and keeping the solutions are represented as **QA** and **A** in Fig. S3, respectively. If $\mathbf{A} = \emptyset$, because the procedure has not converged to an optimum solution, then the procedure is reconfigured again as mentioned in Section S3.4.

S3.7. Agreement with the literature and other methods

DMs make a second test and keep those solutions from **A**, represented as **B** in Fig. S3, that are consistent with the information previously collected from the literature and results obtained with other methods. The procedure of checking the agreement of every solution x is represented as **C** in Fig. S3. If $\mathbf{B} = \emptyset$, and therefore, **A** is composed of solutions that are physically invalid, then the procedure is reconfigured again as mentioned in Section S3.4.

S3.8. Final result

Finally, DMs are in charge of selecting the best solution x from **B** following their expert criteria. Once again, the use of previous analyses, reports or results are of great help in the decision-making.

S3.9. Comments

Three different colors are used for the boxes in Fig. S3. Blue represents those steps in which information is gathered. This information is used by DMs to make informed decisions and configure the procedure strategically. Red represents those steps related to the evolutionary procedure, mainly its configuration and execution. Finally, yellow represents those steps in which the decision-making have a great impact, being crucial the DMs' knowledge as experts in the topic.

S4. Transient fitting with a second order exponential decay function

The three $I_D - t$ current transients shown with symbols in Fig. 5a (also represented in Figs. S4 and S5) can be fitted in the range $500 < t < 1000$ s with a two-term exponential decay function

$$A_k + B_k \exp(-t/\tau_1) + C_k \exp(-t/\tau_2) \tag{S4}$$

with ($k = 1...3$) [3, 11]. In Fig. S4a, the fitting can be seen with solid lines in which A_k, B_k, C_k are extracted independently in each of the three transients. Their values are shown in Table S1. The values of the extracted time

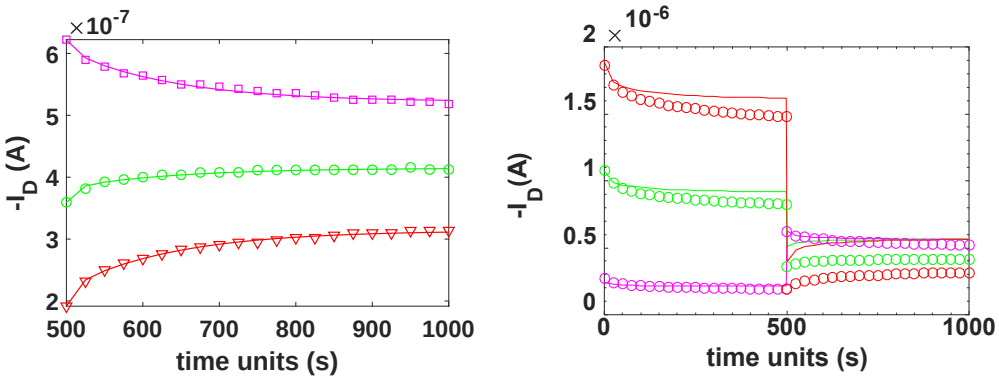

(a) (b)

Figure S4: (a) Fitting with (S4) (lines) of the experimental current transients shown in Fig. 5a (symbols) in the range $500 < t < 1000$ s, the fitting parameters are in Table S1. (b) Comparison of our calculations with our model (solid lines) and the same current transients (symbols) in the range $0 < t < 1000$ s. The model parameters are in Table 1 but with $\tau_1 = 10$ s and $\tau_2 = 140$ s, extracted from the fitting in (a).

Table S1: Values of parameters of the two-term exponential decay function (S4) employed in the fitting of the current transients shown in Fig. S4a in the range $500 < t < 1000$ s.

Variable	$V_G = -10$ V	$V_G = -30$ V	$V_G = -50$ V
A (A)	5.21×10^{-07}	4.14×10^{-07}	3.13×10^{-07}
B (A)	1.70×10^{-08}	-2.31×10^{-08}	-2.95×10^{-08}
τ_1 (s)	$1.00 \times 10^{+01}$	$1.00 \times 10^{+01}$	$1.00 \times 10^{+01}$
C (A)	8.29×10^{-08}	-3.21×10^{-08}	-9.25×10^{-08}
τ_2 (s)	$1.40 \times 10^{+02}$	$1.40 \times 10^{+02}$	$1.40 \times 10^{+02}$

constants are $\tau_1 = 10$ s and $\tau_2 = 140$ s. If these values of τ_1 and τ_2 replace the ones shown in Table 1 and new transients are calculated with our model (1), (3), (6), (12) and (13), (15) and (17), the result can be seen in solid lines in Fig. S4b. This is not a proper fitting because $\tau_1 = 10$ s and $\tau_2 = 140$ s were extracted from a part of the experiment (current transients in the range $500 < t < 1000$ s) and employing that $I_D(t \to \infty) = A_k$ is different for each of the three curves of Fig. S4a. In steady state conditions, $I_D(t \to \infty) = A_k$ should be the same $\forall k = 1...3$, as seen in our calculations of Fig. S4b and imposed in the best fitting shown in Fig. 5a. Conversely, the fitting of the transient data with (S4) imposing A_k to have the same value for the three transient is seen in Fig. S5. As was the case for the previous fitting, this one could not be considered a proper fitting since $\tau_2 = 5.00 \times 10^{+03}$ s might be considered to be out of reasonable limits with regard to the flat area (around 1000 s) seen in Fig 5a (also seen in Figs. S4a and S5).

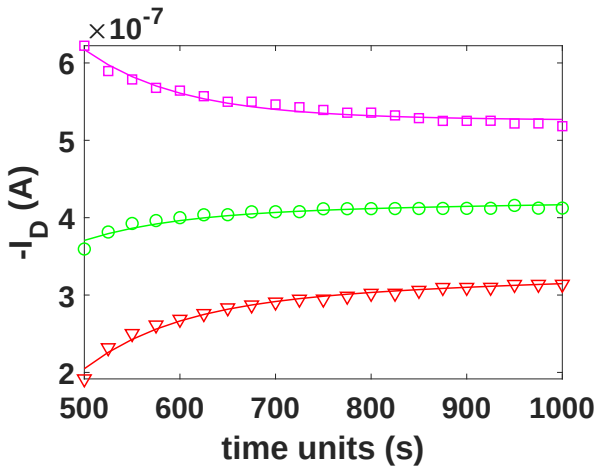

Figure S5: (a) Fitting with (S4) (lines) of the experimental current transients shown in Fig. 5a (symbols) in the range $500 < t < 1000$ s, the fitting parameters are in Table S2.

Table S2: Values of parameters of the second order exponential decay function (S4) employed in the fitting of the current transients shown in Fig. S5 in the range $500 < t < 1000$ s.

Variable	$V_G = -10$ V	$V_G = -30$ V	$V_G = -50$ V
A (A)	5.00×10^{-07}	5.00×10^{-07}	5.00×10^{-07}
B (A)	8.81×10^{-08}	-3.76×10^{-08}	-9.11×10^{-08}
τ_1 (s)	$1.00 \times 10^{+02}$	$1.00 \times 10^{+02}$	$1.00 \times 10^{+02}$
C (A)	2.91×10^{-08}	-9.17×10^{-08}	-2.04×10^{-07}
τ_2 (s)	$5.00 \times 10^{+03}$	$5.00 \times 10^{+03}$	$5.00 \times 10^{+03}$

References

[1] M. Deen, M. Kazemeini, Y. Haddara, J. Yu, G. Vamvounis, S. Holdcroft, W. Woods, Electrical characterization of polymer-based FETs fabricated by spin-coating poly(3-alkylthiophene)s, IEEE Trans. Electron Devices 51 (11) (2004) 1892–1901.

[2] P. López-Varo, J. A. Jiménez Tejada, O. Marinov, J. Carceller, C. Chen, M. Deen, Boundary condition model for the simulation of organic solar cells, Org. Electron. 48 (2017) 85–95.

[3] C. Ucurum, H. Goebel, F. A. Yildirim, W. Bauhofer, W. Krautschneider, Hole trap related hysteresis in pentacene field-effect transistors, Journal of Applied Physics 104 (8) (2008) 084501.

[4] C. Ucurum, Understanding and modeling the hysteresis in current-voltage (I–V) and capacitance-voltage (C–V) characteristics of organic thin-film transistors, Ph.D. thesis, Fakultät für Elektrotechnik der Helmut-Schmidt-Universität/Universität der Bundeswehr Hamburg (2013).

[5] A. Romero, J. González, R. Picos, M. J. Deen, J. A. Jiménez-Tejada, Evolutionary parameter extraction for an organic TFT compact model including contact effects, Org. Electron. 61 (2018) 242 – 253.

[6] A. Cerdeira, M. Estrada, R. García, A. Ortiz-Conde, F. G. Sánchez, New procedure for the extraction of basic a-Si:H TFT model parameters in the linear and saturation regions, Solid-State Electron. 45 (7) (2001) 1077–1080.

[7] O. Marinov, M. J. Deen, C. Feng, Y. Wu, Precise parameter extraction technique for organic thin-film transistors operating in the linear regime, J. Appl. Phys. 115 (3) (2014) 034506.

[8] A. Ortiz-Conde, A. Sucre-González, F. Zárate-Rincón, R. Torres-Torres, R. S. Murphy-Arteaga, J. J. Liou, F. J. García-Sánchez, A review of DC extraction methods for MOSFET series resistance and mobility degradation model parameters, Microelectron. Reliab. 69 (2017) 1–16.

[9] A. Romero, J. González, J. A. Jiménez-Tejada, Constrained Many-Objective Evolutionary Extraction Procedure for an OTFT Compact Model Including Contact Effects, in: 2018 Spanish Conference on Electron Devices (CDE), IEEE, 2018, pp. 1–4.

[10] A. Romero, J. González, M. Deen, J. A. Jiménez-Tejada, Versatile model for the contact region of organic thin-film transistors, Org. Electron. 77 (2020) 105523.

[11] G. Gu, M. G. Kane, J. E. Doty, A. H. Firester, Electron traps and hysteresis in pentacene-based organic thin-film transistors, Applied Physics Letters 87 (24) (2005) 243512.